

Machine learning for structure-property mapping of Ising models: Scalability and limitationsZhongzheng Tian, Sheng Zhang , and Gia-Wei Chern*Department of Physics, University of Virginia, Charlottesville, Virginia 22904, USA*

(Received 20 April 2023; accepted 27 November 2023; published 13 December 2023)

We present a scalable machine learning (ML) framework for predicting intensive properties and particularly classifying phases of Ising models. Scalability and transferability are central to the unprecedented computational efficiency of ML methods. In general, linear-scaling computation can be achieved through the divide-and-conquer approach, and the locality of physical properties is key to partitioning the system into subdomains that can be solved separately. Based on the locality assumption, ML model is developed for the prediction of intensive properties of a finite-size block. Predictions of large-scale systems can then be obtained by averaging results of the ML model from randomly sampled blocks of the system. We show that the applicability of this approach depends on whether the block-size of the ML model is greater than the characteristic length scale of the system. In particular, in the case of phase identification across a critical point, the accuracy of the ML prediction is limited by the diverging correlation length. We obtain an intriguing scaling relation between the prediction accuracy and the ratio of ML block size over the spin-spin correlation length. Implications for practical applications are also discussed. While the two-dimensional Ising model is used to demonstrate the proposed approach, the ML framework can be generalized to other many-body or condensed-matter systems.

DOI: [10.1103/PhysRevE.108.065304](https://doi.org/10.1103/PhysRevE.108.065304)**I. INTRODUCTION**

Machine learning (ML) is a fast-advancing field that has reshaped many industries. ML has achieved surprising success in many real-world problems, including machine vision, speech recognition, and natural language processing. In recent years, numerous successful ML applications in a wide range of disciplines have also led to a paradigmatic shift in scientific research. The remarkable capability of modern ML methods to deduce complex patterns from large datasets has allowed scientists to derive connections between raw data and desired quantities, a task which previously would have been impossible. One of the most important application of ML in materials science is the fast and accurate prediction of material properties from the structural or configurational data [1–9]. Indeed, ML-based modeling of structure-property relationships is expected to open a new avenue for accelerated materials discoveries [10–14].

Similar ML approaches to structure-property modeling also have enormous applications in condensed matter physics [15,16]. A particularly interesting aspect of condensed matter systems is the emergence of complex symmetry-breaking phases or topological orders. The objectives of ML models are to provide proper characterizations of such emergent “structures,” from which accurate predictions about the properties of the system can be made. Of particular interest is the classification of different phases and the identification of phase transitions of many-body systems [17–26]. For example, deep neural networks (NN) have been employed to distinguish the ordered or critical phases from the high-temperature disordered state in various classical spin systems [17,27–32]. With proper feature engineering, ML models have also been developed to capture topologically nontrivial phases or many-body localized states [33–37].

Despite the impressive success of ML models in classifying the various many-body phases, the crucial issue of scalability, which is one of the main motivations for adopting ML approaches, has not been carefully addressed. In most studies mentioned above, the ML models, mostly implemented using deep-learning NNs, are designed for a specific system size and take the processed configuration of the whole system as the input. As a result, a new ML model has to be rebuilt and retrained for different system sizes. Besides the lack of transferability, importantly, such approach cannot be feasibly generalized to realistic systems in the thermodynamic limit. A scalable ML framework is thus required for both numerical and practical applications. Here the scalability refers to the capability of the framework to cope with arbitrary system size without changing the ML structures and parameters, such as the number of layers and neurons in a NN, while maintaining satisfactory performance.

One representative example of scalable ML frameworks is the Behler-Parrinello (BP) type schemes [38,39] for the ML force field models in quantum MD simulations [40–50]. In such approaches, the total energy, which corresponds to the potential energy surface for atoms in the Born-Oppenheimer approximation, is partitioned into local contributions: $E = \sum_i \varepsilon_i$, where ε_i is called the atomic energy associated with the i th atom. The atomic energy is then assumed to depend predominantly on the immediate chemical environment within a length scale to be denoted as r_{BP} . The complex dependence of atomic energy on the local environment is to be approximated by an ML model. It is worth noting that the locality principle, or nearsightedness of electronic matter [51,52], is implicitly employed in this framework. Crucially, the ML model in this scheme has a fixed size which is determined by the linear scale r_{BP} of the input local neighborhood and is independent of the system size to be modeled. As a result, the ML model can be

used in systems of arbitrary large sizes through partitioning. The atomic forces which are crucial to MD simulations are obtained from the derivative of the total energy $\mathbf{F}_i = -\partial E/\partial \mathbf{R}_i$. Similar scalable ML frameworks have also been developed for multi-scale dynamical modeling of condensed-matter lattice models and correlated electron systems [53–58].

Recently, a ML framework similar in spirit to the BP scheme is proposed for efficient prediction of general extensive properties such as energy, entropy, and magnetization of arbitrarily large systems [59–62]. In this approach, dubbed extensive deep-learning NN (EDNN), the system is first partitioned into partially overlapping subdomains, also called “tiles,” of a fixed size. The length scale of the tiles is determined by the locality of the extensive quantity A of interest [59]. The overlap regions are introduced to partially account for the nonlocal effect involved in the determination of the extensive property. Importantly, as in the BP approach, a fixed-size NN model is developed to predict the extensive property A_α of the α th tile, and the extensive property of the whole system is given by the sum of contributions from each tile: $A = \sum_\alpha A_\alpha$. Again, as the NN model is of fixed size, it could be applied to arbitrarily large systems through the partitioning into tiles of the designed size.

It is worth noting that the above BP and EDNN schemes are examples of scalable ML models based on fully connected neural networks. However, scalability can be naturally incorporated into other neural network structures, most notably in models which build on convolutional neural networks (CNNs) [63]. The convolution operation with a finite-sized kernel naturally incorporates the locality principle into the ML structure. Indeed, CNN-based scalable ML spin torque models have recently been developed to enable large-scale dynamical simulations of metallic magnets [58,64]. Convolution operations are also employed in graph neural networks (GNNs) to provide localized mappings of graph elements, thus offering a natural implementation of scalable ML structures. Several recent works have applied GNN to build scalable interatomic potentials for quantum MD simulations [65–68]. Finally, building on transformations of a fixed size Fourier modes, neural operators are yet another scalable neural net architecture [69].

In this paper, we propose a scalable ML framework similar to the BP schemes for identifying phases and phase transitions and, more generally, for predicting intensive properties of a many-body system. We demonstrate our approach using the 2D Ising model as an example. We note that the phase classification is a special case of intensive properties, which denote attributes of a system that is independent of system sizes. Since intensive attributes are spatially nonlocal in nature, their prediction poses great challenges for ML methodology. In our approach, a ML model is first developed to predict the intensive properties of a finite-size block, and the intensive property of the whole system is obtained by averaging over ML predictions of a number of randomly sampled blocks of the system. The ML model here is of a fixed size characterized by the size ℓ of the block, which plays a role similar to the length-scale r_{BP} in BP-type ML models. We further show that the prediction accuracy depends strongly on the ratio of the block size ℓ to the correlation length ξ of the system, underscoring the importance of locality in scalable ML models.

The rest of the paper is organized as follows. A general framework of a scalable NN model for prediction of intensive properties is outlined in Sec. II. ML models are developed for the energy-density prediction and phase classification of the 2D Ising model. A detailed study of the effect of the finite block size on the phase classification accuracy is presented in Sec. III. In particular, we obtain a scaling relation relating the prediction error to the ratio of block size relative to the correlation length. A summary and implications of our results are presented in Sec. IV.

II. SCALABLE ML FRAMEWORK FOR INTENSIVE PROPERTIES

In this section we present a scalable ML framework for predicting intensive properties of a many-body system. A particular application of this ML model is the classification of phases of a many-body system, as phase-labeling is a special intensive property of the system. Indeed, classification has long been a central subject in ML applications. Classification algorithms used in ML utilize input training data for the purpose of predicting the likelihood that a given new data will fall into one of the predetermined categories. However, scalability has not been a focus for computer scientists in traditional vision and audio-based applications of deep-learning. For example, most classification problems in image-processing, e.g., identification of certain objects or shapes in an image, are independent to the physical dimensions of an image. More specifically, the input of a ML model for image processing depends on the number of pixels of a picture, instead of its actual physical dimensions.

Early applications of ML models to classification problems in condensed-matter physics also paid little attention to the issue of scalability. For example, it has been shown that a simple fully connected feed-forward NN with only one hidden layer is able to detect the two phases of the 2D Ising model and accurately reproduce the critical temperature through finite-size extrapolation [17]. Since each node of the input layer corresponds to an Ising spin of the 2D lattice, the size of the input layer depends on the system size. Similar ML approaches have since been developed for phase classification of numerous classical many-body systems [27–32]. However, the architecture of such ML models obviously lacks scalability: ML model developed for a particular system size cannot be directly applied to systems of larger dimensions.

As discussed in Sec. I, linear scalability methods in many-body systems rely on the principle of locality, which means physical properties only depend on configurations of a finite neighborhood. This allows for a divide-and-conquer approach to the computation of the physical properties of interest. Based on this locality principle, here we discuss a scalable ML framework for efficient prediction of intensive properties and particularly phase classification of a many-body system. The limitations of this approach, due to the breakdown of locality, will be discussed in Sec. III. While the formulation presented here can be applied to general many-body systems, for concreteness and as a proof of principle, we demonstrate our approach using the square-lattice ferromagnetic Ising model [70]: $\mathcal{H} = -J \sum_{\langle ij \rangle} \sigma_i \sigma_j$, where $\sigma_i = \pm 1$ represents an Ising spin at site- i , $\langle ij \rangle$ denotes a nearest-neighbor pair, and

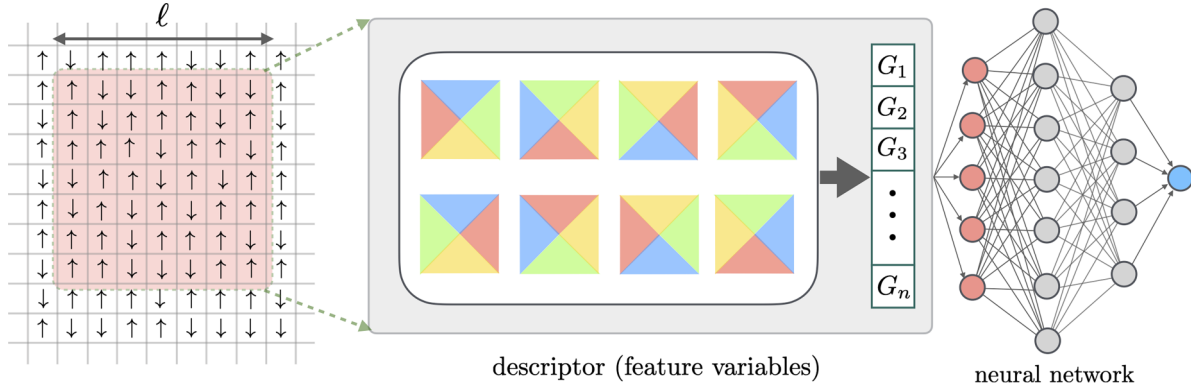


FIG. 1. Machine learning model for phase classification or prediction of other intensive properties of a two-dimensional Ising model. The ML model is composed of two central components: the descriptor and the neural network. The input of the ML model is a square block of Ising spins with a linear size ℓ . The descriptor corresponds to a representation of this spin-block that is invariant with respect to symmetry operations of the D_4 point group of the square lattice. Essentially, the eight symmetry-related configurations are mapped to the same feature variables $\mathbf{G} = (G_1, G_2, G_3, \dots)$, which are then fed to the input layer of the NN. The output node of the NN gives the predicted intensive property.

$J > 0$ is the strength of the ferromagnetic interaction. This canonical spin model exhibits two thermodynamical phases: a high-temperature paramagnet with disordered spins and a long-range ordered ferromagnetic state at low temperatures. A critical point at $T_c \approx 2.269J$ separates the two phases.

Central to our approach is the construction of a ML model which takes a finite block of Ising spins as input and predicts some intensive quantities \mathcal{Q} at the output; see Fig. 1. There are two central components of the ML model: the descriptor and the neural network (NN). The spin configuration within the block is mapped to a set of feature variables $\mathbf{G} = \{G_1, G_2, \dots\}$, also known as a descriptor, which is invariant under the symmetry transformations of the original Hamiltonian. With the symmetrized representation \mathbf{G} as the input, the NN produces the predicted intensive properties at the output nodes. The linear size ℓ of the spin block is a special hyperparameter of the ML model. In particular, ℓ determines the size of the input layer of the NN.

A. Lattice descriptor

The construction of descriptor or feature variables is similar to the so-called image augmentation which is a common technique used to artificially expand the size and diversity of a training dataset by applying various transformations to the original images. These transformations can include rotation, scaling, flipping, translation, or color changes, among others. The goal is to make the model more robust and invariant to these transformations, which helps improve generalization and performance on new, unseen data. For applications to materials science or condensed matter physics, however, even with the augmented dataset, symmetries of the original physical Hamiltonian can only be learned approximately even with the general approximation capability of NNs. In particular, for ML models with output that are invariant under symmetry operations, a proper representation of the input variables should also be invariant with respect to the same symmetry group for consistency. This crucial step of ML models, namely the construction of the proper descriptor, is often referred to as feature engineering [71–76].

Descriptors also play a crucial role in the scalable BP-type ML interatomic potential or force-field models in quantum MD methods. In MD applications, a proper descriptor of the atomic configuration should be invariant under rotational and permutational symmetries, while retaining the faithfulness of the Cartesian representation. Over the past decade, several descriptors have been proposed to represent the atomic or chemical environment. Notably among them are the Coulomb matrix method [71], moment tensor potentials [76], the atom-centered symmetry functions (ACSFs) [38,77], and the group-theoretical bispectrum method [39,73].

For condensed matter systems defined on a lattice, the relevant symmetry operations are internal symmetries of the constituent degrees of freedom and the discrete symmetries of the lattice. Examples of the former are the Z_2 symmetry of Ising variables, $O(2)$ symmetry of XY spins, and so on. For lattice systems, the symmetry of a local neighborhood is described by the point group associated with the site symmetry. A descriptor of lattice models thus should be invariant with respect to both types of symmetry groups. A general theory of descriptors for lattice models has recently been presented in Ref. [78]; several explicit implementations have also been demonstrated for well-known model systems [53–58].

For application to the Ising model, the internal symmetry group of Ising spins is Z_2 while the lattice symmetry is described by the D_4 point group. We first consider invariant representations with respect to the point-group symmetry. Essentially, the goal here is to map the eight Ising configurations related by symmetry operations of the D_4 group, as shown in Fig. 1, to the same feature variables $\mathbf{G} = \{G_\ell\}$. To this end, we employ group-theoretical method to obtain invariant variables of Ising configurations within a block B_α , where α is an index of the block. First, we note that Ising spins $\{\sigma_j\}$ within a given block forms a high-dimensional reducible representation of the D_4 group, which can then be decomposed into fundamental irreducible representations (IR's) of the point group. This decomposition can be highly simplified as the representation matrix is automatically block-diagonalized, with each block corresponding to a fixed distance from the center-site of the block. We use $\mathbf{f}^\Gamma = (f_1^\Gamma, f_2^\Gamma, \dots, f_{D_r}^\Gamma)$ to denote the basis

function of IR of the symmetry-type Γ . For example, four nearest-neighbor Ising spins $\{\sigma_1, \sigma_2, \sigma_3, \sigma_4\}$ form a closed representation, and can be decomposed as $4 = 1A_1 + 1B_1 + 1E$, where $f^{A_1} = \sigma_1 + \sigma_2 + \sigma_3 + \sigma_4$ and so on; more details can be found in the Appendix.

Given these IR coefficients, one immediate class of invariants is their amplitudes $p^\Gamma = |f^\Gamma|^2$, which is called the power spectrum of the representation. However, the descriptor also needs to account for crucial information on the relative phases of different IRs. To capture the phase information, we introduce the concept of reference IR coefficients f_{ref}^Γ , which are obtained by applying similar decomposition procedure to large symmetry-related groups of Ising spins within the block B_α such that they are insensitive to small variations of the neighborhood [78]. Importantly, the relative phase of two IRs can be restored from their respective relative phases $\eta^\Gamma \sim f^\Gamma \cdot f_{\text{ref}}^\Gamma$ to the reference IR. A complete set of invariant feature variables is then given by the power spectrum p^Γ and the phases η^Γ ; see the Appendix for more details. Finally, we note that the power-spectrum obviously is invariant under the Z_2 transformation $\sigma \rightarrow -\sigma$ and $f \rightarrow -f$. The relative phases also remain the same under the Z_2 symmetry as both the IR and the corresponding reference IR change sign. The Z_2 symmetry is automatically preserved in this descriptor.

B. Neural network

Given the invariant representation of the spin block B_α , the corresponding intensive property, let us call it Q , is assumed to depend on the feature variables through a universal function. Specifically, let B_α be the spin configurations within the α th block, the intensive property Q of the block is given by

$$Q_\alpha = Q(B_\alpha) = \hat{f}(\mathbf{G}_\alpha), \quad (1)$$

where $\mathbf{G}_\alpha = \{G_1(B_\alpha), G_2(B_\alpha), \dots\}$ denote feature variables built from the α th block, and the ‘‘universal’’ function $\hat{f}(\cdot)$ (universal in the sense of a given Hamiltonian) is to be approximated by a deep neural network. Because of the discrete nature of Ising spins, we include a number of convolutional layers to better represent the discretized input feature variables. CNNs are a class of neural networks that utilize the shared-weight architecture of convolutional filters, also called kernels, to process input features. One of the main advantages of CNN is that they can effectively handle discrete data by smoothly sliding the filters over the input, which leads to the emergence of translational equivariant responses. In other words, the CNN’s ability to extract local features across multiple spatial positions allows it to recognize patterns in the input data regardless of their location, making it a powerful tool for image and signal processing tasks. This property enables CNN to capture the structural characters of the images and other 2D/3D objects.

The output of the CNN is then fed into a fully connected feed-forward NN, which performs a sequence of transformations. Specifically, for the m th layer, the neuron processes the activation $\mathbf{a}^{(m-1)}$ from the previous $(m-1)$ th layer through weight and bias parameters: $\mathbf{a}^{(m)} = \mathbf{A}(\mathbf{w}^{(m-1)}\mathbf{a}^{(m-1)} + \mathbf{b}^{(m-1)})$, where \mathbf{A} is an array of identical activation functions, $\mathbf{w}^{(m-1)}$ is the weight of the $(m-1)$ th layer, and $\mathbf{b}^{(m-1)}$ is the bias of the $(m-1)$ th layer. Finally,

the node at the end of the feed-forward NN is the predicted intensive property Q_α . These NN parameters \mathbf{w} and \mathbf{b} of both CNN and feed-forward NN are essentially fitting parameters for the high-dimensional function f_{ML} , which are determined through training with stochastic gradient descent.

C. Training of the ML model

The NN model can be optimized through standard supervised training algorithms. For example, for a spin block described by feature variables \mathbf{G} , the loss function can be defined as the mean square error (MSE) $\mathcal{L} = |\hat{f}(\mathbf{G}) - f_{\text{ML}}(\mathbf{G})|^2$. In this approach, each spin block is treated as independent training dataset. However, for highly inhomogeneous systems, large fluctuations of block-spin configuration are expected. Such situations occur, for example, in spin systems close to a critical point. To better account for local variations of spin-blocks, here we propose a training scheme shown schematically in Fig. 2, which is similar in spirit to the BP-type ML models for quantum MD simulations. The training dataset is obtained from a system of linear size L which could be much larger than the block size ℓ . We partition the large Ising system into $M \sim (L/\ell)^2$ blocks, each is labeled by B_α , where the index $\alpha = 1, 2, \dots, M$; see Fig. 2(a). Importantly, the training is based on averaged predictions from these M blocks. For example, we consider the following MSE loss function for a given snapshot of the system

$$\mathcal{L} = \left| \hat{Q} - \frac{1}{M} \sum_{\alpha=1}^M f_{\text{ML}}(\mathbf{G}_\alpha) \right|^2, \quad (2)$$

where \hat{Q} is the exact intensive property of the whole $L \times L$ system, and \mathbf{G}_α is the feature variables for the α th block of the snapshot. For phase classification problem where $Q = 1$ or 0 corresponds to whether the system is in a specific phase or not, a cross entropy can be used for the loss function.

With either MSE or cross entropy loss functions, as demonstrated in Fig. 2(a), one can view the training process as the optimization of a super-neural net build from M copies of the same NN shown in Fig. 1. Finally, standard stochastic gradient descent method with back propagation is used to optimize the ML model from multiple snapshots of the whole system. It is worth noting that the above scheme is different from ML training based on M independent blocks. With loss function determined from the averaged predictions from all blocks, the optimization of the ML model is forced to take into account the potentially diverse block-spin configurations within the same system.

We emphasize again the similarity of our approach to BP-type ML structures discussed above. By partitioning the total energy of the system into local energies $E = \sum_{i=1}^N \varepsilon_i$, where N is the number of atoms, the local energy associated with the i th atom is assumed to depend on its immediate chemical environment, also denoted as C_i , through a universal function, i.e., $\varepsilon_i = \epsilon_{\text{ML}}(C_i)$. This universal function $\epsilon_{\text{ML}}(\cdot)$ is similarly to be approximated by a ML model. For MD applications, one is mostly interested in atomic forces, which are given by the derivatives, $\mathbf{F}_i^{\text{ML}} = -\partial E / \partial \mathbf{R}_i$, and are dependent indirectly on the universal function. Importantly, the loss function for a given snapshot of atoms is based on

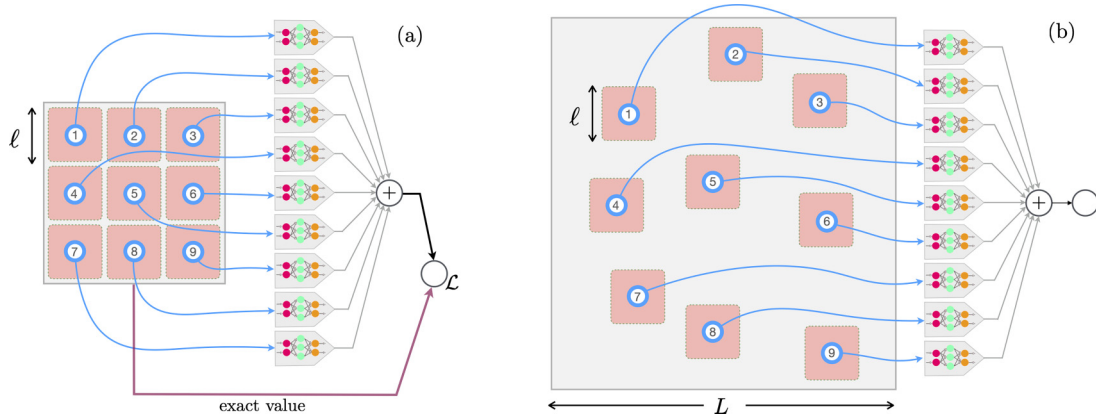


FIG. 2. A scalable ML approach relies on the partitioning of the system into finite-size blocks that can be solved individually. The presumably time-consuming calculation of some physical properties of the block of linear size ℓ is encoded in the ML model, which is implemented using the multi-layer NN here. Panel (a) shows a schematic of the training process. The loss function \mathcal{L} quantifies the difference between the exact value and the average of the ML predictions from each block. For application of the ML framework to large systems, one can design the partitioning such that the blocks cover the whole system. However, for extremely large system $L \gg \ell$, or experimental data where the system approaches the thermodynamic limit, a practical approach is to randomly select a large number of blocks to represent the system, as shown in panel (b). The estimation of the physical property is again the average of ML prediction from all blocks.

prediction difference of total energy and individual forces, e.g., $\mathcal{L} = \sum_i |\hat{\mathbf{F}}_i - \mathbf{F}_i^{\text{ML}}|^2 + r|\hat{E} - \sum_i \varepsilon_i|^2$, where the $\hat{\mathbf{F}}_i$ and \hat{E} denote the forces and total energy, respectively, obtained from, e.g., DFT calculations, and coefficient r specifies the relative ratio of energy constraints compared to that of forces. The ML model $\varepsilon_{\text{ML}}(\cdot)$, which determines both the forces \mathbf{F}_i^{ML} and local energies, is optimized from the minimization of this loss function defined on the whole atomic system.

Once the ML model is optimized, its utilization for predicting intensive properties of a much larger system is based on a random sampling method. As shown in Fig. 2(b), a number N_{sample} of $\ell \times \ell$ blocks are randomly selected from the whole system. Let $Q_\alpha = f_{\text{ML}}(\mathbf{G}_\alpha)$ be the ML prediction of the α th block, the intensive property of the system is approximated by averaging over these local predictions

$$\bar{Q} = \frac{1}{N_{\text{sample}}} \sum_{\alpha=1}^{N_{\text{sample}}} f_{\text{ML}}(\mathbf{G}_\alpha). \quad (3)$$

One can also obtain an estimate of the prediction error from the standard deviation of the local predictions:

$$\sigma_Q = \left[\frac{1}{N_{\text{sample}}} \sum_{\alpha=1}^{N_{\text{sample}}} (f_{\text{ML}}(\mathbf{G}_\alpha) - \bar{Q})^2 \right]^{1/2}. \quad (4)$$

For large number of sampling blocks, the prediction accuracy can be improved by the average \bar{Q} . Moreover, the standard deviation σ_Q provides information of the intrinsic fluctuations of the intensive properties within the system measured based on the length scale ℓ associated with the ML model.

D. ML prediction of energy density

As a demonstration, here we first apply the above approach to the prediction of the energy density $\rho_E = E/N$ of the 2D Ising model, where $E = -J \sum_{\langle ij \rangle} \sigma_i \sigma_j$ is the total energy of the system and $N = L^2$ is the total number of spins. It is worth noting that the energy calculation in short-range Ising model,

or most classical short-range spin models, is linear-scaling and can be done rather efficiently. However, the computational time is still of the order of $\mathcal{O}(N)$, which will become infeasible in the thermodynamic limit. However, the time complexity of the ML method scales as $\mathcal{O}(N_{\text{sample}})$, which is controlled by the number of sampling blocks. Moreover, the ML approach also offers a more efficient calculation of energy density for models with long-range interactions or quantum systems where the energy calculation requires time-consuming many-body methods.

The construction of both the descriptor and the neural network (NN) model was implemented using the PyTorch library. To accelerate the training process of the machine learning (ML) model, multiple graphics processing units (GPUs) were employed in PyTorch. The training dataset was composed of 40 000 Ising configurations of a lattice with linear size $L = 320$, while an additional 8 000 Ising configurations were used for validation. The temperature values of the training and validation datasets were evenly distributed across 40 different temperatures ranging from $T_{\text{low}} = 1.2J$ to $T_{\text{high}} = 3.6J$. The ML models were constructed using two block sizes $\ell = 32$ and 64 as the input data. Finally, the model is trained using the Adam optimizer [79] with adaptive learning rate of 0.001 and 500 epochs.

Figures 3(a) and 3(b) show the ML-predicted energy density versus temperature curves for an $L = 320$ Ising system based on block sizes $\ell = 32$ and 64 , respectively. The results from the Monte Carlo (MC) simulations are also shown for comparison. While the overall ML predictions agree well with the MC results, a systematic discrepancy can be seen from the figures: the ML models tend to overestimate the energy density above the critical temperature and to underestimate the energy below T_c ; see also the comparison of ML predictions against the energy density from MC simulations in Figs. 3(c) and 3(d). This systematic errors become more noticeable for ML models with a smaller block size ℓ .

It should be noted that, while computing the energy of a given spin-block is almost trivial especially for short-ranged

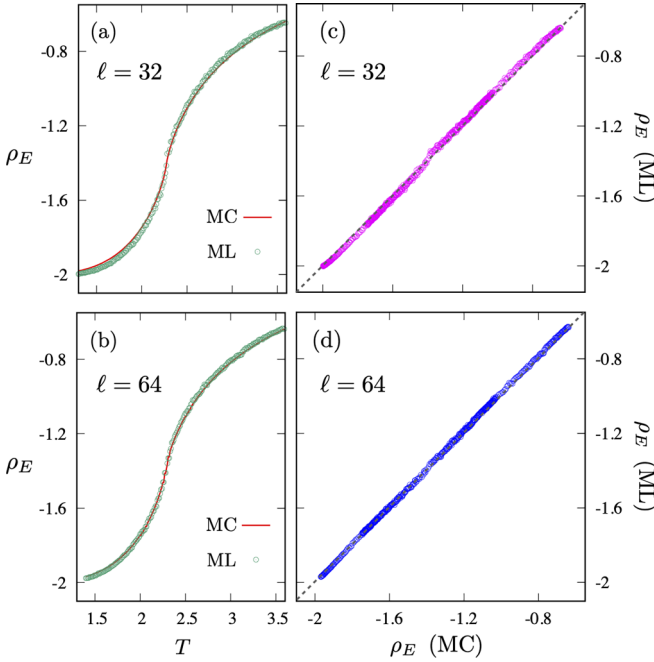


FIG. 3. Left panels show the energy density ρ_E of the 2D Ising model as a function of temperature obtained from Monte Carlo (MC) simulations and ML predictions with block size (a) $\ell = 32$ and (b) $\ell = 64$. The right panels show the comparison of energy density predicted by ML models versus that obtained from MC simulations again for two different block sizes (c) $\ell = 32$ and (d) $\ell = 64$.

spin models, our objective here is to predict the intensive property of the whole system through a window of linear size ℓ . This is also the source of the prediction errors observed in Fig. 3. The discrepancy is also due to the requirement that same ML model is trained to predict the intensive property of both high- and low-temperature phases, including the critical regime around T_c . Indeed, excellent prediction accuracy can be achieved if the ML model is restricted to either the high-temperature paramagnet or the long-range ordered phase at low T . The highly inhomogeneous spin states in the vicinity of the critical point introduces significant uncertainties in the training of finite-size ML models, giving rise to the systematic errors in both phases. Intuitively, to model spin configurations in the critical regime which comprises diverse spin configurations characterized by large length scales, the ML model is forced to compromise its prediction capability of both the high and low temperature phases. A more systematic analysis of prediction error and its relation to the diverging correlation length at the critical point are discussed in the next section.

III. CORRELATION LENGTH AND LIMITATION OF SCALABILITY

Although interactions of most physical systems are local and characterized by microscopic length scales of the order of lattice constants, emergent structures of the system are often described by length scales, denoted as ξ for convenience, that are often much larger than the microscopic one. More importantly, the locality of intensive quantities \mathcal{Q} which depend on the emergent structures is controlled such new length scales

ξ . For example, while spin-spin interactions in the standard Ising model are restricted to nearest neighbors, the spatial fluctuations of spin configurations are determined by the correlation length ξ of the system. In general, the correlation length characterizes the exponential decay of the structural correlation function

$$C(\mathbf{r}) \sim \exp(-|\mathbf{r}|/\xi). \quad (5)$$

Importantly, the length scale ξ is often not a fundamental parameter of the Hamiltonian, but is controlled by external parameters such as temperature or magnetic field.

The effects of correlation length on the performance of ML model with a finite block size ℓ can be intuitively understood from the two snapshots in Fig. 4. The squares in both panels correspond to the spin-block for the input of the ML model. For systems at high temperatures, as exemplified by Fig. 4(a), the length scales of spatial fluctuations or inhomogeneity is much smaller than the block size, $\xi \ll \ell$. Consequently, spin configurations sampled by a given block are good representatives of the whole system. As a result, ML predictions based on even one block could be accurate in this limit.

However, larger and larger spin clusters start to emerge as system approaches the critical temperature T_c , as shown in Fig. 4(b). The average linear size of spin clusters is again characterized by the correlation length ξ . When this length scale is greater than the block size, $\xi \gtrsim \ell$, an individual spin block is expected to exhibit rather distinct spin configurations. As a result, each block only captures partial information of the larger-scale structures of the system. By taking into account all spin blocks of the whole system in the optimization of the ML model, the training scheme outlined in Fig. 2(a) with a loss function of Eq. (2) aims to strike a balance between spatial features of length scale ℓ . The ML prediction shown in Fig. 2(b) can be viewed as attempting to assemble information contained in several small pictures of size ℓ to form a big picture at the length scale of ξ . However, due to the ambiguities and tradeoff between different blocks during the training, the accuracy of ML prediction is significantly hampered in the $\xi \gg \ell$ limit.

To examine quantitatively the effects of a diverging correlation length on the ML prediction accuracy, here we develop a ML model for the phase classification of the 2D Ising model. To this end, a deep-learning NN with one nonreducing and five reducing fully connected layers was constructed. The NN produces a single digit \mathcal{Y} at the output layer such that $\mathcal{Y} = 0$ and 1 corresponds to the low- T ferromagnetic order and the paramagnetic phase at high temperatures, respectively. As discussed above, the ML model is designed to provide an accurate approximation for the structure-property mapping $\mathcal{Y} = f_{\text{ML}}(\mathbf{G})$ of the spin block, where $\mathbf{G} = \{G_1, G_2, \dots\}$ are symmetry-invariant feature variables built from spin configuration of the block discussed above. A binary cross entropy (BCE) loss function was employed for the optimization of NN model. Specifically, let $\bar{\mathcal{Y}}_m$ denotes the ML prediction averaged over all blocks of the m th snapshot of an $L \times L$ Ising system, and $\hat{\mathcal{Y}}_m$ be the true value of the corresponding phase, the BCE loss function is defined as

$$\mathcal{L} = -\frac{1}{\mathcal{N}} \sum_{m=1}^{\mathcal{N}} [\hat{\mathcal{Y}}_m \log(\bar{\mathcal{Y}}_m) + (1 - \hat{\mathcal{Y}}_m) \log(1 - \bar{\mathcal{Y}}_m)], \quad (6)$$

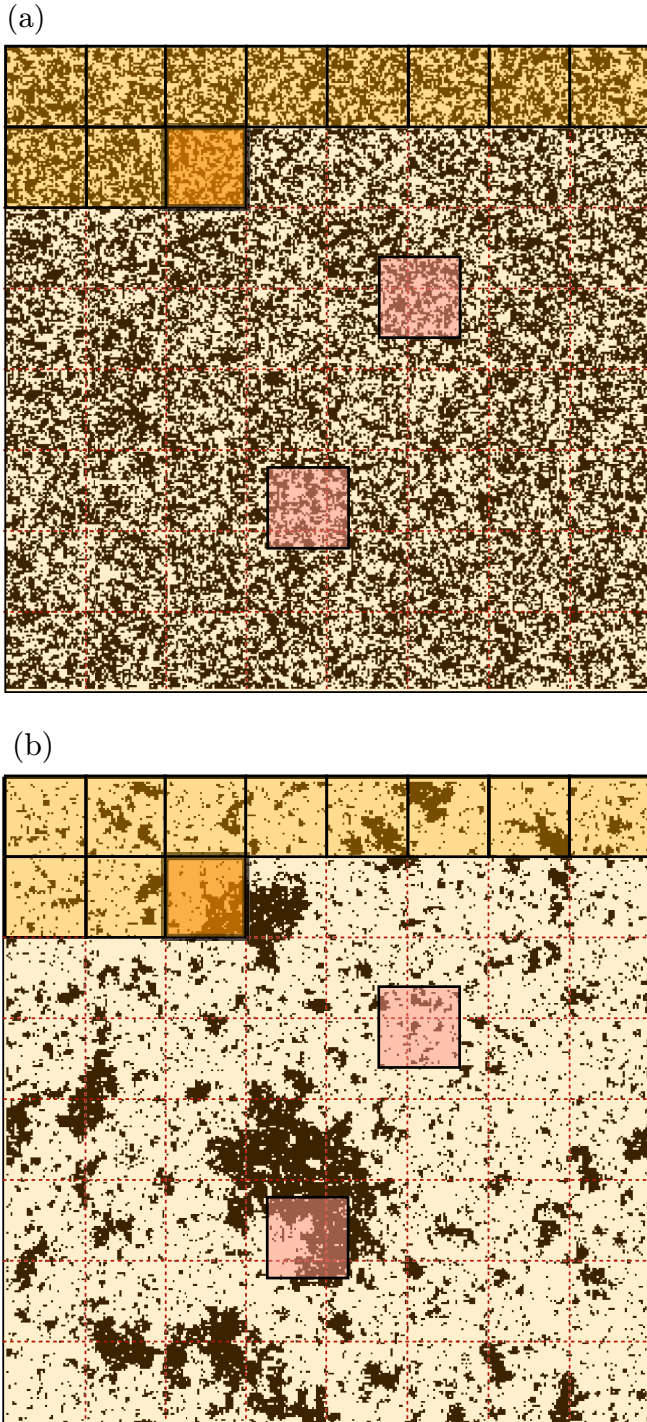


FIG. 4. Comparison of the block size ℓ and the correlation length ξ of the 2D Ising model at (a) $T = 4.2J$, which is representative of the high-temperature paramagnetic phase, and (b) $T = 2.28J$ close to the critical point $T_c \approx 2.269J$.

where \mathcal{N} is the number of snapshots used in the training. For the phase classification, $\mathcal{N} = 50\,000$ Ising configurations from Monte Carlo simulations on a $L = 320$ system were used to train the NN model, with an additional 10 000 snapshots reserved for validation. The datasets were obtained from MC simulations over a range of temperatures similar to that in the ML model for energy density. An Adam optimizer with

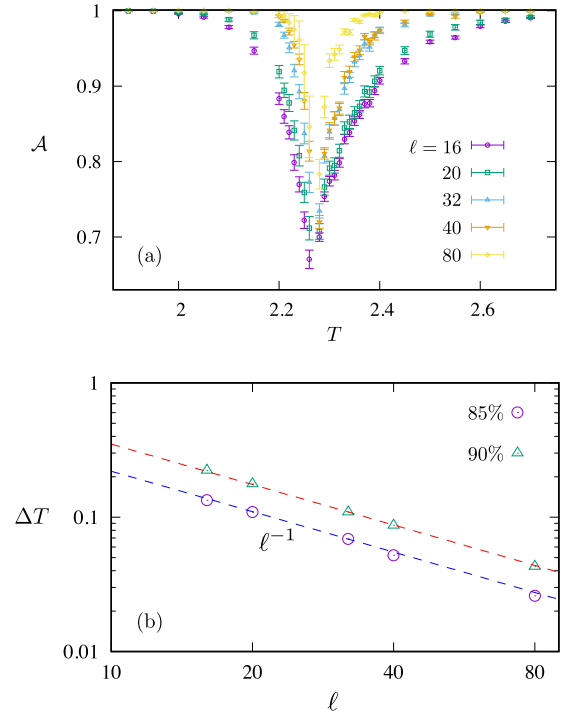


FIG. 5. (a) Accuracy \mathcal{A} of ML phase classification versus temperature for ML models of different block sizes ℓ . (b) The temperature window $\Delta T = T_+^* - T_-^*$ where the classification accuracy \mathcal{A} drops below 85% and 90% versus the block size ℓ . The dashed lines indicate the power-law behavior $\Delta T \sim \ell^{-1}$.

a global learning rate of 0.001 is used. A dropout layer is added before the output layer with a dropout probability set to 0.2.

Figure 5(a) shows the prediction accuracy \mathcal{A} versus temperature for ML models of different block sizes ℓ . The prediction accuracy here is defined as the ratio of successful predictions over the total number of test data. Overall, as expected, the classification accuracy is better for ML models with larger block size. Moreover, while relatively high classification accuracy can be reached in both the high- and low- T phases, especially for ML models with larger ℓ , the prediction accuracy is significantly reduced in the vicinity of the critical temperature T_c for all ML models. More quantitatively, we define T_{\pm}^* as the temperatures at which the prediction accuracy drops below a certain threshold; the subscript \pm refers to the high- and low-temperature side of the critical point, respectively. The temperature window $\Delta T = T_+^* - T_-^*$ within which the accuracy is below threshold 85% and 90% is shown in Fig. 5(b) as a function of ML block size. Interestingly, while this temperature span ΔT indeed is reduced with increasing block size, we find that its decrease can be very well described by a power-law behavior $\Delta T \sim \ell^{-1}$.

To understand this result, we note that the divergence of the correlation length as a many-body system approaches the critical point T_c is described by a power law with an exponent ν :

$$\xi(T) \sim \frac{1}{|T - T_c|^\nu}. \quad (7)$$

For the 2D Ising model, this exponent can be obtained from Onsager's exact solution, which gives $\nu = 1$ [70]. As discussed above, when this correlation length becomes much greater than the size ℓ of spin block used for ML model, spin configurations sampled by each block fail to capture the larger spin structure. Consequently, an ML model with input block size ℓ will start to break down when the correlation length reaches the block size

$$\xi^* = \xi(T^*) \sim \ell. \quad (8)$$

Using the power-law relation for $\xi(T)$, one obtains the threshold temperatures on both sides of the critical point

$$T_{\pm}^* \sim T_c \pm \text{const} \times \ell^{-1/\nu}. \quad (9)$$

Defining the temperature span of reduced classification accuracy as $\Delta T = T_+^* - T_-^*$, we thus obtain the following power-law relation

$$\Delta T \sim \ell^{-1/\nu}. \quad (10)$$

For 2D Ising model with $\nu = 1$, the above result is consistent with our numerical simulation shown in Fig. 5(b).

In fact, the above result suggests a scaling relation for the prediction accuracy similar to the finite-size scaling relations for a continuous phase transition. For example, the order-parameter m of the 2D Ising model exhibits a scaling relation with the system size: $m \sim L^{\beta/\nu} \Psi(L/\xi)$ in the critical regime; here $\Psi(x)$ is a universal function and exponent $\beta = 1/8$ for the 2D Ising model [70]. To apply similar analysis to our case, first the role of system size L is now replaced by the block size ℓ . Moreover, as the accuracy tends to 1 at both high and low temperatures, this suggests a scaling relation for the prediction error which is defined as the difference $\varepsilon = (1 - \mathcal{A})$. Assuming that the system size L for generating either the training and testing data is much larger than both the correlation length and block size (which is not true when $T \sim T_c$), the prediction error should depend on the ratio ℓ/ξ of the only two relevant length scales. This suggests the following scaling relation:

$$\varepsilon = (1 - \mathcal{A}) \sim \ell^{-\theta} \Phi(\ell/\xi), \quad (11)$$

where $\Phi(x)$ is a quasiuniversal function which depends on the implementation of ML models, and θ is an exponent characterizing the improvement of classification accuracy with increasing block size. This scaling relation is indeed confirmed by our block-size scaling of ML predictions. As shown in Fig. 6, by plotting $(1 - \mathcal{A})\ell^\theta$ at the y axis and $(\ell/\xi)^{1/\nu} \sim (T - T_c)\ell^{1/\nu}$ at the x axis, rather nice data point collapsing was obtained using exponent $\theta = 0.12$ and $\nu = 1$ from the 2D Ising model. The scaling relation Eq. (11) shows that, in addition to the rather weak power-law dependence $\ell^{-\theta}$ on the block size, the ML prediction error depends strongly on the ratio of the block size relative to the correlation length. This dependence also underpins the power-law behavior Eq. (10) for the temperature span with reduced prediction accuracy.

Finally, we note that the scaling relation Eq. (11) needs to be modified when the correlation length ξ grows to be greater than the finite system size L used in simulations, which happens in the very vicinity of the critical point. In this $\xi \gg L$ limit, the prediction accuracy of our ML scheme depend on both the block size and the system size, not necessarily on the dimensionless ratio ℓ/L . Specifically, we expect the prediction

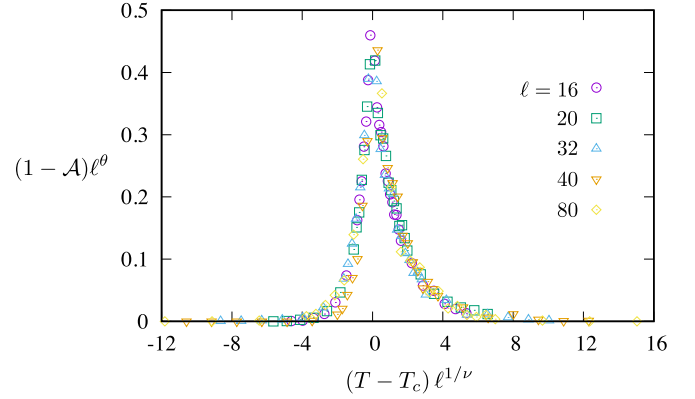


FIG. 6. Block size scaling analysis of the ML prediction accuracy. The figure shows $(1 - \mathcal{A})\ell^\theta$ versus $(T - T_c)\ell^{1/\nu}$ from prediction results with different block size ℓ . The exponents $\nu = 1$ is from the 2D Ising model and $\theta = 0.12$. The rather nice data collapsing suggests a relation $(1 - \mathcal{A})\ell^\theta = F[(T - T_c)\ell^{1/\nu}]$, where the function $F(x)$ is related to the scaling function in Eq. (11) as $\Phi(x) = F(x^{1/\nu})$.

error to be dependent on both ratios: ℓ/ξ and L/ξ . First, for a given system size L , based on arguments discussed above, increasing block size ℓ is expected to result in a better accuracy. However, even for a fixed block size ℓ , the prediction accuracy can be enhanced by a larger system size L . This is because the characteristic features are now determined by L (finite-size effect) in the large ξ limit. As a result, a larger L could allow for more intrinsic features of the system to be present in the system, which can then be better sampled by the ML blocks.

IV. SUMMARY AND OUTLOOK

We have presented a scalable ML framework, which is a natural generalization of previous ML-based approaches to structure-property relationships, for the prediction of intensive properties of many-body systems. In particular, our approach focuses on ML models which can be directly applied to much larger systems without either rebuilding or retraining the model. Specifically, an ML model is developed to produce an estimate of intensive properties based on input of a finite block, characterized by linear size ℓ , of the system. The training of the ML model is carried out based on dataset of a larger system of linear size L such that the combined prediction of ML model on the $(L/\ell)^d$ blocks is used to optimization parameters of the ML model, where d is the spatial dimension. By including contributions of all blocks of a configuration as a batch for the training, the optimization of the ML model takes into account the structural variations of individual blocks. Application of the trained ML model to large-scale systems is via a random sampling method, i.e., prediction of system-wise intensive properties is obtained by averaging over ML predictions from a large number of randomly selected blocks.

The two-dimensional Ising model, which is widely used as a benchmark system for ML applications to statistical mechanics and many-body systems, is used to demonstrate our approach. ML models are built for energy-density prediction and phase classification. We show that the breakdown of locality in the vicinity of the critical point leads to uncertainties

of ML training, which in turn results in systematic errors for the prediction of energy density. Nonetheless, the systematic errors can be reduced with increasing block size ℓ of the ML model. Furthermore, we show that deterioration in the phase classification accuracy is characterized by the condition $\xi \gtrsim \ell$. The prediction error ε is found to exhibit a scaling relation which depends strongly on the ratio of block size to the correlation length.

Our proposed ML framework is similar to other ML modeling of structure-property relationship. The crucial difference, due to the demand of scalability, is that the ML model in our approach is to provide a mapping from local structures characterized by linear size ℓ to global (intensive) properties of the whole system. The feasibility of this scheme relies on the locality of a many-body system, which is also key to almost all linear-scaling methods. In general, the principle of locality means that local physical quantities only depend on configurations of the immediate surrounding. In our case, however, the locality assumption means that intensive properties of a system can be inferred from finite-size structures locally. Accurate predictions can be achieved only when the linear size ℓ of local structures to be modeled by the fixed-size ML model is greater than the structural correlation length ξ of the system. Interestingly, this means that ML models for accurate phase classification are possible for systems exhibiting first-order phase transitions, since correlation length remains finite during such discontinuous transitions.

While our scalable ML modeling of the structure-property relationships is based on supervised learning, it is worth noting that phase classification, which is a special case of intensive property prediction, can be achieved using other ML approaches including unsupervised learning methods [26,80]. In particular, building on the analogy between the renormalization group (RG) process and deep learning, neural network models, such as super-resolution CNN [81] and restricted Boltzmann machines (RBM) [82–84], have been developed to accurately identify the phase transition temperature and predict critical properties such as critical exponents. However, as in the RG methods, these ML approaches are focused more on the critical regime of a second-order phase transition. They could not give quantitative predictions well outside the critical regime of a continuous transition, or for a first-order phase transition. Our proposed scalable ML framework, however, aims at a quantitative structure-property mapping when the correlation length ξ is comparable to the ML block size.

For quantitative predictions of continuous properties, such as energy density, the intrinsic symmetry of the system can be properly incorporated into ML models via a symmetry-invariant descriptor. Explicit demonstration of how D_4 symmetry is exactly included in the ML prediction of energy density of the 2D Ising model is presented in the Appendix. Essentially, we show that ML models without any symmetrization preprocessing of Ising configurations give rise to the so-called equivariant errors, which means the ML model predicts different energies for Ising configurations which are related by D_4 symmetry operations. However, we also note that incorporation of symmetry-invariant descriptor has very limited improvement in the performance of phase classifications. This is understandable because the distinguishing of the two phases relies more on the very different spin-spin

correlations than on whether symmetry is properly preserved in the ML model.

For predictions of electronic properties such as energy gap, magnetic susceptibility, or electrical conductivity, although the input to ML models is the directly measurable atomic structures, it should be noted that the relevant correlation length ξ is determined by the electron systems. A representative example is the BP-type ML interatomic potential models for quantum molecular dynamics simulations. In these applications, ML models are designed to predict a local atomic energy based on the neighborhood atomic configurations. Yet, the size of the neighborhood depends on the electronic correlation functions, instead of atomic configurations. As the electron correlation decays exponentially for gapped systems, ML models with large enough ℓ are expected to provide an accurate approximation for such systems.

ACKNOWLEDGMENTS

The authors are grateful for useful discussions with Puhang Zhang and Chen Cheng. This work was supported by the U.S. Department of Energy Basic Energy Sciences under Award No. DE-SC0020330. The authors also acknowledge the support of Advanced Research Computing Services at the University of Virginia.

APPENDIX: DESCRIPTOR FOR SQUARE-LATTICE ISING MODEL

As discussed in Sec. II, the goal of a descriptor is to preserve lattice symmetry of the original lattice Hamiltonian in the ML model. A general theory and several specific implementations of descriptors in condensed matter systems, especially for lattice models, have recently been presented in Ref. [78]. In particular, the group-theoretical bispectrum method was generalized to systematically generate feature variables that are invariant under symmetry operations of the on-site point group [53,78]. Here, we apply this method to develop a descriptor for the 2D Ising model. There are two sets of discrete symmetries in the square-lattice Ising model: one is the Z_2 symmetry of Ising spins which physically is related to the time-reversal symmetry, and the second is the D_4 point-group symmetry of the $\ell \times \ell$ spin block on a square lattice. To account for the Z_2 symmetry, one approach is to first build bilinear forms of Ising spins $b_{jk} = \sigma_j \sigma_k$, also known as bond variables, within the spin block. These bilinear variables b_{jk} , which are invariant under Z_2 transformation $\sigma_i \rightarrow -\sigma_i$, are then used as building blocks for the lattice descriptor.

Here, however, we employ a different and simpler approach by constructing invariants of the point-group symmetry first. The Z_2 symmetry will be automatically included in the reference method to be discussed below. To this end, we first note that the Ising spins in an $\ell \times \ell$ block form a high-dimensional reducible representation of the D_4 group. For convenience, we use B_α to denote spin configurations in the α th block. The first step of finding invariants under site symmetry is to decompose B_α into irreducible representations (IRs) of the symmetry group. This decomposition is considerably simplified due to the lattice geometry. Essentially, since the distance between a neighborhood site- j and the center

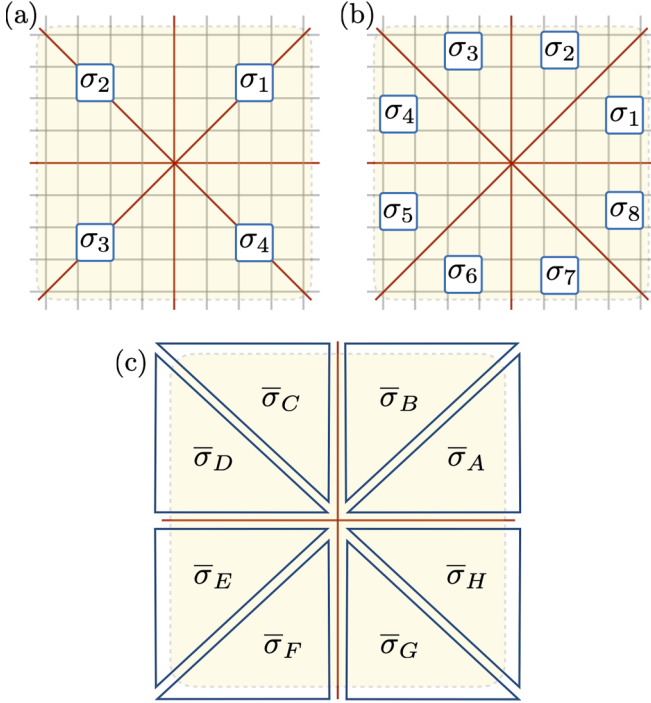


FIG. 7. Schematic diagrams of (a) four-site and (b) eight-site groups within a spin block. Panel (c) shows the eight triangular domains used to compute the coefficients of reference IRs.

site- i is invariant under operations of the D_4 group, the resultant matrix representation is thus block-diagonalized, with each block corresponding to a group of Ising spins sharing the same distance to the center. In the case of D_4 , the size of these invariant spin groups is either 4 or 8; see Figs. 7(a) and 7(b). The four-site block can be decomposed as $4 = 1A_1 \oplus 1B_1 \oplus 1E$. The expansion coefficients of each IR are

$$\begin{aligned} f_{A_1} &= \sigma_a + \sigma_b + \sigma_c + \sigma_d, \\ f_{B_1} &= \sigma_a - \sigma_b + \sigma_c - \sigma_d, \\ f_E &= (\sigma_a - \sigma_c, \sigma_b - \sigma_d). \end{aligned} \quad (A1)$$

The decomposition of the eight-site block is $8 = 1A_1 + 1B_1 + 1A_2 + 1B_2 + 2E$, with the following coefficients for each IR:

$$\begin{aligned} f_{A_1} &= \sigma_a + \sigma_b + \sigma_c + \sigma_d + \sigma_e + \sigma_f + \sigma_g + \sigma_h, \\ f_{A_2} &= \sigma_a - \sigma_b + \sigma_c - \sigma_d + \sigma_e - \sigma_f + \sigma_g - \sigma_h, \\ f_{B_1} &= \sigma_a - \sigma_b - \sigma_c + \sigma_d + \sigma_e - \sigma_f - \sigma_g + \sigma_h, \\ f_{B_2} &= \sigma_a + \sigma_b - \sigma_c - \sigma_d + \sigma_e + \sigma_f - \sigma_g - \sigma_h, \\ f_{(E,1)} &= (\sigma_a + \sigma_b - \sigma_e - \sigma_f, -\sigma_c - \sigma_d + \sigma_g + \sigma_h), \\ f_{(E,2)} &= (\sigma_c - \sigma_d - \sigma_g + \sigma_h, \sigma_a - \sigma_b - \sigma_e + \sigma_f). \end{aligned} \quad (A2)$$

As the spin block B_α contains several such four-site or eight-site groups, we expect same IRs appear multiple times in the overall decomposition of the spin block. In the following, we label each IR in the decomposition of B_α as $\Gamma = (T, r)$, where $T = A_1, A_2, \dots$ denotes the symmetry type of the IR, and r indicates different occurrence of the same IR. For convenience, we arrange the expansion coefficients of an IR Γ into a vector $\mathbf{f}_\Gamma = (f_{\Gamma,1}, f_{\Gamma,2}, \dots, f_{\Gamma,n_\Gamma})$, where n_Γ is the dimension of Γ .

The power spectrum of the representation are given by the amplitudes of the IR coefficients

$$p_\Gamma = |\mathbf{f}_\Gamma|^2. \quad (A3)$$

Since the power spectrum coefficients are obviously invariant under symmetry transformations, they can be used as feature variables for the ML models. However, a descriptor composed only of power spectrum is incomplete since the relative phases between different IRs are ignored. This also means that descriptor contains spurious symmetries as the transformation of each IR is independent of each other without the phase information. A complete set of feature variables can be obtained from the bispectrum coefficients $b_{\Gamma_1, \Gamma_2, \Gamma_3}$, which are triple products of the expansion coefficients $\mathbf{f}_{\Gamma_{1,2,3}}$ based on the Clebsch-Gordan coefficients of the point group. Intuitively, they can be viewed as the analog of scalar triple product of three-dimensional vectors. Not only are the bispectrum coefficients invariant under symmetry transformations, they can also be used to faithfully reconstruct the original disorder configuration [73,74].

However, a descriptor based on all the bispectrum coefficients is in fact over-complete as many of them are redundant. Moreover, since the dimension of most IRs of point groups is rather small, the number of bispectrum coefficients is often a very large number, which makes the implementation infeasible. Instead, here we employ the method of reference IR discussed in Ref. [78] to retain the phase information. The central idea is to first construct an eight-dimensional representation of the spin block B_α based on average of Ising spins over symmetry-related finite regions. As shown in Fig. 7(c), an example is given by $(\bar{\sigma}_A, \bar{\sigma}_B, \dots, \bar{\sigma}_H)$ where $\bar{\sigma}_K = \frac{1}{|K|} \sum_{i \in K} \sigma_i$ is given by the average of all Ising variables within region- K .

The decomposition of this eight-dimensional representation $\bar{\sigma}_K$ then gives coefficients $f_{A_1}^*, f_{A_2}^*, \dots, f_E^*$ for each symmetry type. These coefficients \mathbf{f}_T^* are termed the reference IR coefficients. For each IR, an effective phase can be defined by the following inner product:

$$\eta_\Gamma = (\mathbf{f}_\Gamma \cdot \mathbf{f}_{T_r}^*) / |\mathbf{f}_\Gamma| |\mathbf{f}_{T_r}^*|, \quad (A4)$$

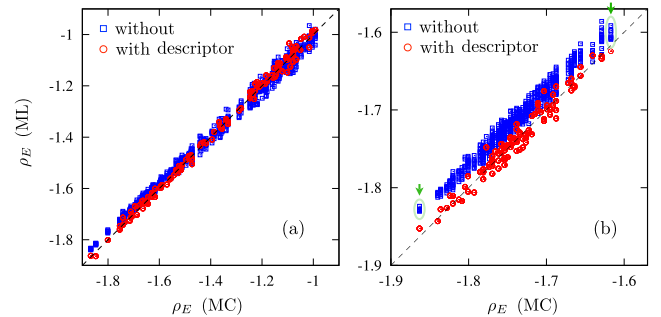


FIG. 8. Energy density ρ_E of 2D Ising model predicted by ML models, with and without the descriptor, versus exact value for spin configurations sampled by Monte Carlo simulations. Panel (a) shows the comparison over a wide range of temperatures, while panel (b) highlights the low-temperature region. As shown by the two examples highlighted by arrows in panel (b), the spreading of predicted energies for exact the same Ising configuration indicates the equivariant error of the ML model without symmetry-invariant descriptor.

where T_Γ is the symmetry type of IR Γ . The phase η_Γ , which is an inner product of two IR coefficients, is naturally invariant with respect to symmetry operations. More importantly, by including η_Γ in the descriptor, the relative phases between different f_Γ are now be inferred through the intermediate reference IR coefficients. Finally, since the IR coefficients f are linear combinations of Ising spins, they acquire a negative sign $f \rightarrow -f$ under the Z_2 transformation. However, both the power spectrum Eq. (A3) and the relative phases Eq. (A4) are bilinear product of the IR coefficients, the resultant descriptor is automatically invariant with respect to the Z_2 symmetry of the Ising model.

To demonstrate how the D_4 symmetry is properly incorporated in the ML model with the descriptor, we compare its performance with a ML model but with the unprocessed Ising spins within a block of same size ℓ as the input. In particular,

here we focus on the prediction of energy density as discussed in Sec. II D. We first prepare a test set of Ising configurations obtained from Monte Carlo simulations. Then for each of the Ising state in the test set, we include all eight configurations which are related by the symmetry operations of the D_4 group in the expanded dataset. The predicted energy density ρ_E from ML models with and without the symmetry-invariant descriptor for the expanded test dataset is shown in Fig. 8. For the ML model with symmetry-invariant descriptor, the model predicts exactly the same energy for the eight symmetry-related Ising configurations as expected. However, the ML model without the descriptor, namely using the unprocessed block Ising spins as input, exhibits noticeable so-called equivariant errors, which manifests as a spreading of predicted energies for exactly the same Ising configurations as highlighted in Fig. 8(b).

-
- [1] J. Jung, J. I. Yoon, H. K. Park, J. Y. Kim, and H. S. Kim, An efficient machine learning approach to establish structure-property linkages, *Comput. Mater. Sci.* **156**, 17 (2019).
- [2] S. S. Schoenholz, E. D. Cubuk, D. M. Sussman, E. Kaxiras, and A. J. Liu, A structural approach to relaxation in glassy liquids, *Nat. Phys.* **12**, 469 (2016).
- [3] Z. Fan, J. Ding, and E. Ma, Machine learning bridges local static structure with multiple properties in metallic glasses, *Mater. Today* **40**, 48 (2020).
- [4] K. Swanson, S. Trivedi, J. Lequieu, K. Swanson, and R. Kondor, Deep learning for automated classification and characterization of amorphous materials, *Soft Matter* **16**, 435 (2020).
- [5] P. Hundi and R. Shahsavari, Deep learning to speed up the development of structure-property relations For hexagonal boron nitride and graphene, *Small* **15**, 1900656 (2019).
- [6] R. Abdusalamov, P. Pandit, B. Milow, M. Itskov, and A. Rege, Machine learning-based structure-property predictions in silica aerogels, *Soft Matter* **17**, 7350 (2021).
- [7] V. Bapst, T. Keck, A. Grabska-Barwinska, C. Donner, E. D. Cubuk, S. S. Schoenholz, A. Obika, A. W. R. Nelson, T. Back, D. Hassabis, and P. Kohli, Unveiling the predictive power of static structure in glassy systems, *Nat. Phys.* **16**, 448 (2020).
- [8] H. Zhang, Z. Guo, H. Hu, G. Zhou, Q. Liu, Y. Xu, Q. Qian, and D. Dai, A novel structure-property relationship model based on machine learning, *Model. Simul. Mater. Sci. Eng.* **28**, 035002 (2020).
- [9] G. L. W. Hart, T. Mueller, C. Toher, and S. Curtarolo, Machine learning for alloys, *Nat. Rev. Mater.* **6**, 730 (2021).
- [10] R. Ramprasad, R. Batra, G. Pilania, A. Mannodi-Kanakithodi, and C. Kim, Machine learning in materials informatics: Recent applications and prospects, *npj Comput. Mater.* **3**, 54 (2017).
- [11] K. T. Butler, D. W. Davies, H. Cartwright, O. Isayev, and A. Walsh, Machine learning for molecular and materials science, *Nature (London)* **559**, 547 (2018).
- [12] J. Schmidt, M. R. G. Marques, S. Botti, and M. A. L. Marques, Recent advances and applications of machine learning in solid-state materials science, *npj Comput. Mater.* **5**, 83 (2019).
- [13] D. Morgan and R. Jacobs, Opportunities and challenges for machine learning in materials science, *Annu. Rev. Mater. Res.* **50**, 71 (2020).
- [14] J. E. Saal, A. O. Oliynyk, and B. Meredig, Machine learning in materials discovery: Confirmed predictions and their underlying approaches, *Annu. Rev. Mater. Res.* **50**, 49 (2020).
- [15] G. Carleo, I. Cirac, K. Cranmer, L. Daudet, M. Schuld, N. Tishby, L. Vogt-Maranto, and L. Zdeborová, Machine learning and the physical sciences, *Rev. Mod. Phys.* **91**, 045002 (2019).
- [16] E. Bedolla, L. C. Padierna, and R. Castaneda-Priego, Machine learning for condensed matter physics, *J. Phys.: Condens. Matter* **33**, 053001 (2021).
- [17] J. Carrasquilla and R. G. Melko, Machine learning phases of matter, *Nat. Phys.* **13**, 431 (2017).
- [18] L. Wang, Discovering phase transitions with unsupervised learning, *Phys. Rev. B* **94**, 195105 (2016).
- [19] S. J. Wetzel, Unsupervised learning of phase transitions: From principal component analysis to variational autoencoders, *Phys. Rev. E* **96**, 022140 (2017).
- [20] A. Bohrdt, C. S. Chiu, G. Ji, M. Xu, D. Greif, M. Greiner, E. Demler, F. Grusdt, and M. Knap, Classifying snapshots of the doped Hubbard model with machine learning, *Nat. Phys.* **15**, 921 (2019).
- [21] G. Torlai and R. G. Melko, Learning thermodynamics with Boltzmann machines, *Phys. Rev. B* **94**, 165134 (2016).
- [22] Q. Wei, R. G. Melko, and J. Z. Chen, Identifying polymer states by machine learning, *Phys. Rev. E* **95**, 032504 (2017).
- [23] E. P. L. van Nieuwenburg, Y. H. Liu, and S. D. Huber, Learning phase transitions by confusion, *Nat. Phys.* **13**, 435 (2017).
- [24] J. S. Salcedo-Gallo, C. C. Galindo-Gonzalez, E. Restrepo-Parra, Deep learning approach for image classification of magnetic phases in chiral magnets, *J. Magn. Magn. Mater.* **501**, 166482 (2020).
- [25] K. Ch'ng, J. Carrasquilla, R. G. Melko, and E. Khatami, Machine learning phases of strongly correlated fermions, *Phys. Rev. X* **7**, 031038 (2017).
- [26] W. Hu, R. R. P. Singh, and R. T. Scalettar, Discovering phases, phase transitions, and crossovers through unsupervised machine learning: A critical examination, *Phys. Rev. E* **95**, 062122 (2017).
- [27] C. Wang and H. Zhai, Machine learning of frustrated classical spin models. I. Principal component analysis, *Phys. Rev. B* **96**, 144432 (2017).

- [28] M. Beach, A. Golubeva, and R. Melko, Machine learning vortices at the Kosterlitz-Thouless transition, *Phys. Rev. B* **97**, 045207 (2018).
- [29] I. A. Iakovlev, O. M. Sotnikov, and V. V. Mazurenko, Supervised learning approach for recognizing magnetic skyrmion phases, *Phys. Rev. B* **98**, 174411 (2018).
- [30] V. K. Singh and J. H. Han, Application of machine learning to two-dimensional Dzyaloshinskii-Moriya ferromagnets, *Phys. Rev. B* **99**, 174426 (2019).
- [31] D. Wang, S. Wei, A. Yuan, F. Tian, K. Cao, Q. Zhao, Y. Zhang, C. Zhou, X. Song, D. Xue, and S. Yang, Machine learning magnetic parameters from spin configurations, *Adv. Sci.* **7**, 2000566 (2020).
- [32] F. A. Gómez Albarracín and H. D. Rosales, Machine learning techniques to construct detailed phase diagrams for skyrmion systems, *Phys. Rev. B* **105**, 214423 (2022).
- [33] Y. Zhang and E.-A. Kim, Quantum loop topography for machine learning, *Phys. Rev. Lett.* **118**, 216401 (2017).
- [34] F. Schindler, N. Regnault, and T. Neupert, Probing many-body localization with neural networks, *Phys. Rev. B* **95**, 245134 (2017).
- [35] Y.-T. Hsu, X. Li, D.-L. Deng, and S. D. Sarma, Machine learning many-body localization: Search for the elusive nonergodic metal, *Phys. Rev. Lett.* **121**, 245701 (2018).
- [36] D.-L. Deng, X. Li, and S. Das Sarma, Machine learning topological states, *Phys. Rev. B* **96**, 195145 (2017).
- [37] J. Venderley, V. Khemani, and E.-A. Kim, Machine learning out-of-equilibrium phases of matter, *Phys. Rev. Lett.* **120**, 257204 (2018).
- [38] J. Behler and M. Parrinello, Generalized neural-network representation of high-dimensional potential-energy surfaces, *Phys. Rev. Lett.* **98**, 146401 (2007).
- [39] A. P. Bartók, M. C. Payne, R. Kondor, and G. Csányi, Gaussian approximation potentials: The accuracy of quantum mechanics, without the electrons, *Phys. Rev. Lett.* **104**, 136403 (2010).
- [40] Z. Li, J. R. Kermode, and A. De Vita, Molecular dynamics with on-the-fly machine learning of quantum-mechanical forces, *Phys. Rev. Lett.* **114**, 096405 (2015).
- [41] V. Botu, R. Batra, J. Chapman, and R. Ramprasad, Machine learning force fields: Construction, validation, and outlook, *J. Phys. Chem. C* **121**, 511 (2017).
- [42] Y. Li, H. Li, F. C. Pickard IV, B. Narayanan, F. G. Sen, M. K. Chan, S. K. Sankaranarayanan, B. R. Brooks, and B. Roux, Machine learning force field parameters from *ab initio* data, *J. Chem. Theory Comput.* **13**, 4492 (2017).
- [43] J. S. Smith, O. Isayev, and A. E. Roitberg, ANI-1: An extensible neural network potential with DFT accuracy at force field computational cost, *Chem. Sci.* **8**, 3192 (2017).
- [44] L. Zhang, J. Han, H. Wang, R. Car, and E. Weinan, Deep potential molecular dynamics: A scalable model with the accuracy of quantum mechanics, *Phys. Rev. Lett.* **120**, 143001 (2018).
- [45] J. Behler, Perspective: Machine learning potentials for atomistic simulations, *J. Chem. Phys.* **145**, 170901 (2016).
- [46] V. L. Deringer, M. A. Caro, and G. Csányi, Machine learning interatomic potentials as emerging tools for materials science, *Adv. Mater.* **31**, 1902765 (2019).
- [47] F. Noé, A. Tkatchenko, K.-R. Müller, and C. Clementi, Machine learning for molecular simulation, *Annu. Rev. Phys. Chem.* **71**, 361 (2020).
- [48] R. T. McGibbon, A. G. Taube, A. G. Donchev, K. Siva, F. Hernández, C. Hargus, K.-H. Law, J. L. Klepeis, and D. E. Shaw, Improving the accuracy of Moller-Plesset perturbation theory with neural networks, *J. Chem. Phys.* **147**, 161725 (2017).
- [49] H. Suwa, J. S. Smith, N. Lubbers, C. D. Batista, G.-W. Chern, and K. Barros, Machine learning for molecular dynamics with strongly correlated electrons, *Phys. Rev. B* **99**, 161107(R) (2019).
- [50] T. Mueller, A. Hernandez, and C. Wang, Machine learning for interatomic potential models, *J. Chem. Phys.* **152**, 050902 (2020).
- [51] K. Walter, Density functional and density matrix method scaling linearly with the number of atoms, *Phys. Rev. Lett.* **76**, 3168 (1996).
- [52] E. Prodan, and K. Walter, Nearsightedness of electronic matter, *Proc. Natl. Acad. Sci. USA* **102**, 11635 (2005).
- [53] J. Ma, P. Zhang, Y. Tan, A. W. Ghosh, and G.-W. Chern, Machine learning electron correlation in a disordered medium, *Phys. Rev. B* **99**, 085118 (2019).
- [54] Y.-H. Liu, S. Zhang, P. Zhang, T.-K. Lee, and G.-W. Chern, Machine learning predictions for local electronic properties of disordered correlated electron systems, *Phys. Rev. B* **106**, 035131 (2022).
- [55] P. Zhang, P. Saha, and G.-W. Chern, Machine learning dynamics of phase separation in correlated electron magnets, [arXiv:2006.04205](https://arxiv.org/abs/2006.04205).
- [56] P. Zhang and G.-W. Chern, Arrested phase separation in double-exchange models: Large-scale simulation enabled by machine learning, *Phys. Rev. Lett.* **127**, 146401 (2021).
- [57] S. Zhang, P. Zhang, and G.-W. Chern, Anomalous phase separation in a correlated electron system: Machine-learning enabled large-scale kinetic Monte Carlo simulations, *Proc. Natl. Acad. Sci. USA* **119**, e2119957119 (2022).
- [58] X. Cheng, S. Zhang, P. C. H. Nguyen, S. Azarfar, G.-W. Chern, S. S. Baek, Convolutional neural networks for large-scale dynamical modeling of itinerant magnets, *Phys. Rev. Res.* **5**, 033188 (2023).
- [59] K. Mills, K. Ryczko, I. Luchak, A. Domurad, C. Beeler, and I. Tamblin, Extensive deep neural networks for transferring small scale learning to large scale systems, *Chem. Sci.* **10**, 4129 (2019).
- [60] N. Saraceni, S. Cantori, and S. Pilati, Scalable neural networks for the efficient learning of disordered quantum systems, *Phys. Rev. E* **102**, 033301 (2020).
- [61] P. Mujal, A. M. Miguel, A. Polls, B. Juliá-Díaz, and S. Pilati, Supervised learning of few dirty bosons with variable particle number, *SciPost Phys.* **10**, 073 (2021).
- [62] H. Jung, S. Stocker, C. Kunkel, H. Oberhofer, B. Han, K. Reuter, and J. T. Margraf, Size-extensive molecular machine learning with global representations, *Chem. Syst. Chem.* **2**, e1900052 (2020).
- [63] R. Venkatesan and B. Li, *Convolutional Neural Networks in Visual Computing: A Concise Guide* (CRC Press, Boca Raton, FL, 2017).
- [64] Y. Miyazaki, Equivariant neural networks for spin dynamics simulations of itinerant magnets, *Mach. Learn.: Sci. Technol.* **4**, 045006 (2023).
- [65] C. W. Park, M. Kornbluth, J. Vandermause, C. Wolverton, B. Kozinsky, and J. P. Mailoa, Accurate and scalable graph neural

- network force field and molecular dynamics with direct force architecture, *npj Comput. Mater.* **7**, 73 (2021).
- [66] S. Batzner, A. Musaelian, L. Sun, M. Geiger, J. P. Mailoa, M. Kornbluth, N. Molinari, E. E. Smidt, and B. Kozinsky, E(3)-equivariant graph neural networks for data-efficient and accurate interatomic potentials, *Nat. Commun.* **13**, 2453 (2022).
- [67] K. T. Schütt, O. T. Unke, and M. Gastegger, Equivariant message passing for the prediction of tensorial properties and molecular spectra, in *Proceedings of the 38th International Conference on Machine Learning*, PMLR 139, 9377 (2021).
- [68] M. Haghightalari, J. Li, X. Guan, O. Zhang, A. Das, C. J. Stein, F. Heidar-Zadeh, M. Liu, M. Head-Gordon, L. Bertels, H. Hao, I. Leven, and T. Head-Gordon, NewtonNet: A Newtonian message passing network for deep learning of interatomic potentials and forces, *Dig. Discov.* **1**, 333-343 (2022).
- [69] N. Kovachki, Z. Li, B. Liu, K. Azizzadenesheli, K. Bhattacharya, A. Stuart, and A. Anandkumar, Neural operator: Learning maps between function spaces with applications to PDEs, *J. Mach. Learn. Res.* **24**, 1-97 (2023).
- [70] B. McCoy and T. Wu, *The Two-Dimensional Ising Model* (Harvard University Press, Cambridge, MA, 1973).
- [71] M. Rupp, A. Tkatchenko, K.-R. Müller, and O. A. von Lilienfeld, Fast and accurate modeling of molecular atomization energies with machine learning, *Phys. Rev. Lett.* **108**, 058301 (2012).
- [72] L. M. Ghiringhelli, J. Vybiral, S. V. Levchenko, C. Draxl, and M. Scheffler, Big data of materials science: Critical role of the descriptor, *Phys. Rev. Lett.* **114**, 105503 (2015).
- [73] A. P. Bartók, R. Kondor, and G. Csányi, On representing chemical environments, *Phys. Rev. B* **87**, 184115 (2013).
- [74] R. Kondor, A novel set of rotationally and translationally invariant features for images based on the noncommutative bispectrum, [arXiv:cs/0701127](https://arxiv.org/abs/cs/0701127).
- [75] L. Himanen, M. O. J. Jäger, E. V. Morooka, F. F. Canova, Y. S. Ranawat, D. Z. Gao, P. Rinke, and A. S. Foster, DSCRIBE: Library of descriptors for machine learning in materials science, *Comput. Phys. Commun.* **247**, 106949 (2020).
- [76] A. V. Shapeev, Moment tensor potentials: A class of systematically improvable interatomic potentials, *Multiscale Model. Simul.* **14**, 1153 (2016).
- [77] J. Behler, Atom-centered symmetry functions for constructing high-dimensional neural network potentials, *J. Chem. Phys.* **134**, 074106 (2011).
- [78] P. Zhang, S. Zhang, and G.-W. Chern, Descriptors for machine learning model of generalized force field in condensed matter systems, [arXiv:2201.00798](https://arxiv.org/abs/2201.00798).
- [79] D. P. Kingma and J. Ba, Adam: A method for stochastic optimization, [arXiv:1412.6980](https://arxiv.org/abs/1412.6980).
- [80] R. Zhang, B. Wei, D. Zhang, J.-J. Zhu, and K. Chang, Few-shot machine learning in the three-dimensional Ising model, *Phys. Rev. B* **99**, 094427 (2019).
- [81] S. Efthymiou, M. J. S. Beach, and R. G. Melko, Super-resolving the Ising model with convolutional neural networks, *Phys. Rev. B* **99**, 075113 (2019).
- [82] F. D'Angelo and L. Böttcher, Learning the Ising model with generative neural networks, *Phys. Rev. Res.* **2**, 023266 (2020).
- [83] S. S. Funai and D. Giataganas, Thermodynamics and feature extraction by machine learning, *Phys. Rev. Res.* **2**, 033415 (2020).
- [84] E. de Mello Koch, R. de Mello Koch, and L. Cheng, Is deep learning a renormalization group flow? *IEEE Access* **8**, 106487 (2020).